J Nanostruct 16(4): 5383-5397, Autumn 2026

RESEARCH PAPER

Tuning Microstructure and Magnetic Properties of M-Type Calcium Hexaferrite Nanoparticles via Magnesium Substitution

Zahraa Jabbar Hamakhan [1], Sarah Abbas Jasim [1], Roaa Ramadhan Ahmed [2], Ali Mustafa Mohammad [3], Fatima Yassen Mohammed [1], Noor Adnan Abdulsattar [4], Duaa Nassif Jassim [4]*

[1] *Department of Physics, College of Science, University of Diyala, Diyala 32001, Iraq*

[2] *Department of Physiology and Medical Physics, College of Medicine, University of Diyala, Diyala, 32001, Iraq*

[3] *Department of Physics, College of Education, University of Garmian, Kalar 46021, Iraq*

[4] *Department of Mathematics, Al-Miqdad College of Education, University of Diyala, Diyala 32001, Iraq*

ARTICLE INFO

Article History:
Received 02 July 2026
Accepted 10 September 2026
Published 01 October 2026

Keywords:
Calcium hexaferrite
Magnetic characteristics
Raman Spectra
Sol-gel auto combustion
XRD

ABSTRACT

The influence of Mg^{2+} substitution M-type hexaferrites on their structural and magnetic properties still warrants further comprehensive investigation. This study is performed systematically to understand the effect of Mg in M-type calcium hexaferrite $Ca_{1-x}Mg_xFe_{12}O_{19}$ ($0.00 \le x \le 0.10$) were prepared by sol–gel auto-combustion technique. The XRD pattern verified the formation of single phase and high crystallinity of a hexagonal form of magnetoplumbite. The ionic radius difference of Ca^{2+} and Mg^{2+} ions brought lattice strain, resulting in the decrease in crystallite size from 71.44 nm to 65.79 nm upon Mg substitution but the lattice parameters remained nearly unchanged as α= 5.892-5.897 Å and c= 23.168-23.182 Å. The typical vibrational modes of M-type hexaferrite were confirmed using Raman spectroscopy of which the peaks showed slight shifts and increased in intensity with successful incorporation of Mg ions and local lattice distortion. The FE-SEM images showed that the morphological changes from quasi-spherical grains to platelets and polyhedrons were found in the particles as the concentration of Mg increased. EDX spectra verified that the particles consisted of only Ca, Mg, Fe and O elements. Magnetic measurements demonstrated enhanced soft magnetic behavior, where the saturation magnetization (M_s) increased from 1.030 to 1.637 emu/g and remanent magnetization (M_r) increased from 0.337 to 0.776 emu/g, while coercivity (H_c) decreased significantly from 400.274 to 128.087 Oe. The squareness ratio (M_r/M_s) ranged from 0.327 to 0.474. Mg substitution in calcium hexaferrite enhances its structural and magnetic properties for microwave absorption, electromagnetic shielding, and high-frequency applications.

How to cite this article
J. Hamakhan Z, A. Jasim S, R. Ahmed R, et al. Tuning Microstructure and Magnetic Properties of M-Type Calcium Hexaferrite Nanoparticles via Magnesium Substitution. J Nanostruct, 2026; 16(4):5383-5397. DOI: 10.22052/JNS.2026.04.073

INTRODUCTION

Magnetic materials have an extremely wide variety of industrial and domestic applications, and are a very important part of everyday life. These are applied for the manufacture of industrial equipment and the development of technology [1, 2]. Magnetite is widely available, is the strongest magnetic material known on earth

* *Corresponding Author Email: zahraa.jabbar@uodiyala.edu.iq*

and is an iron ore composed of iron oxide, called ferrites [3, 4]. There are several groups of magnetic ceramic materials, among which the ferrites are presented which are subdivided into four groups: orthoferrites, spinels, garnets and hexaferrites [5]. Hexaferrite materials are hard magnetic materials, studied and known for their convenient properties in the last few decades, compared to the other counterparts. High Curie temperature, have great chemical stability, adjustable magneto crystalline anisotropy, are easy to manufacture, have high magnetic saturation and coercivity, and corrosion resistance [6]. Based on their crystal structure, and chemical composition, M-type hexagonal ferrites ($AFe_{12}O_{19}$), where A represents Ba, Sr, Pb and Ca [7] are suitable for magnetic fluids, medical supply, preservation of medicaments materials in an organism, and hyperthermia of the malignant cells, very suitable materials for the high frequency circuits and operating devices [8]. They can also be used as magnetic recording media for perpendicular magnetic recording, and microwave absorbers [9]. The excellent biological compatibility of the other base compositions - alkaline-earth hexaferrites - over calcium hexaferrites has led to their extensive use in medical applications [10]. A M-type crystal structure is hexagonal and it is composed of 38 oxygen and 24 Ferric ions. In this structure ferric (Fe^{3+}) ions occupy five different interstitial sites in the unit cell, such have three octahedral sites (12k ↑, 2a↑, $4f_2$ ↓), one tetrahedral ($4f_1$ ↓) and one trigonal bipyramidal (2b ↑) site [11]. The substitutions of M-type calcium hexagonal ferrites are achieved to enhance the specific properties of the materials and investigation results have revealed that substitutions can alter the crystallographic, magnetic and electrical properties of the materials [12, 13]. These hexagonal ferrites have properties that depend on the substituted the divalent ions of calcium ions have different positions in the structure [14, 15]. The different factors affecting the properties of this M-type hexaferrite are concentration [16] type of replacement [17], method of synthesis [18], calcination temperature and time [19], metal nitrate to fuel ratio [20], type of fuel [21], pH of solution [22], etc. Several methods have been used for the synthesis of ferrite nanoparticles, such as the coprecipitation method [23], solid-state method [24], hydrothermal synthesis [25], Pechini method [26], sol–gel auto-combustion method [27], and etc. Previous studies on the substitution of secondary and tertiary ions in hexaferrite lattices demonstrated significant variations in structural, magnetic, and electrical characteristics. In a study conducted by Deshpande et al. [28], on Zr-Co substituted $CaFe_{12}O_{19}$ within the compositional range x = 0-4, the saturation magnetization decreased from 0.4975 to 0.1195 emu/g, followed by an increase to 0.1985 emu/g at x = 4. In parallel, the coercivity declined from 875 G to 25 G and subsequently rose to 125 G at x = 4. These changes were attributed to the occupation of Fe^{3+} sublattices by diamagnetic ions. Kakul et al., [29] reported that Sm^{3+} substitution in $CaFe_{12}O_{19}$ increased Ms from 25 to 44 emu/g and reduced Hc from 3.3 to 2.33 kOe, attributed to lattice expansion and enhanced Fe^{3+} sublattice interactions. The materials were shown to have promising magnetic characteristics for storage applications. Ijaz et al., [30] showed that Cu and Dy co-doped M-Type $Ca_{1-x}Cu_xFe_{12-x}Dy_xO_{19}$ (x=0.0, 0.05, 0.10, 0.15, 0.20). The sample with the best magnetic properties is $Ca_{0.85}Cu_{0.15}Fe_{11.85}Dy_{0.15}O_{19}$ with M_s = 35.738 emu/g, $m_B(\mu_B)$ = 6.732B, M_r= 20.430 emu/g, H_c = 3.15 kOe, and M_r/M_s = 0.572. All samples were excellent candidates for use in magnetic devices due to their high M_r/M_s values. The effect of doping on the magnetic features of M-type hexa-ferrites has made them useful in numerous applications, such as high-performance self-biased circulators, magnetic filters, and storage devices. demonstrating that dual-ion substitution tunes anisotropy.

Mawaheb et al. [31] investigated aluminium-substituted calcium–lanthanum M-type hexaferrite with the chemical composition $Ca_{0.5}La_{0.5}Fe_{12-x}Al_xO_{19}$ (x = 0.00, 0.04, 0.08, 0.12, and 0.16). Vibrating sample magnetometer (VSM) analysis showed that the saturation magnetization (M_s) and remanent magnetization (M_r) decreased to 17.01 emu g^{-1} and 10.66 emu g^{-1}, respectively, whereas the coercivity increased to 2.165 kOe as the Al^{3+} substitution level reached x = 0.16. This behavior was attributed to the enhancement of magnetocrystalline anisotropy caused by the incorporation of non-magnetic Al^{3+} ions. Ali [11]. synthesized Co-substituted M-type strontium hexaferrite, $Sr_{1-x}Co_xFe_{12}O_{19}$ (x = 0.00, 0.25, 0.50, 0.75), using the sol–gel auto-combustion method and confirmed ferromagnetic behavior for all samples. The magnetic parameters showed a systematic decrease with increasing Co^{2+} content,

where the saturation magnetization (M_s) decreased from 63.50 to 26.99 emu/g, the remanent magnetization (M_r) decreased from 36.01 to 14.04 emu/g, and the coercivity (H_c) reduced from 4051 to 2571 Oe. This reduction in magnetic properties indicates a progressive weakening of the superexchange interactions within the M-type hexaferrite structure due to Co substitution. Based on these results, the synthesized material demonstrated promising characteristics for magnetic applications. Subsequently, Kumar et al. [32] synthesized Eu–Ti co-doped M-type calcium hexaferrite, $Ca_{1-x}Eu_xFe_{12-y}Ti_yO_{19}$ ($0.00 \leq x, y \leq 0.07$), using the solid-state reaction method.The structure of the synthesized material was found to be M-type hexagonal structure using XRD and Raman spectroscopy, along with the presence of a negligible amount of α-Fe_2O_3 as an impurity. The grain size was found to be in the range of 1.65-2.26 µm using the field emission scanning electron microscopy and the elemental composition and oxidation state was confirmed by EDX and HRXPS analysis. The magnetic properties were measured, and the results revealed that there was variation in coercivity (H_c), remanent magnetization (M_r) and saturation magnetization (M_s) as well as the ratio of remanence to saturation magnetization ($M_r/M_s \leq 0.5$), which showed the presence of significant inter-grain interactions and the suitability of the prepared materials for use in high-frequency devices and high-density magnetic recording applications. In the present study, Mg-substituted calcium hexaferrite powders with the composition $Ca_{1-x}Mg_xFe_{12}O_{19}$ (x = 0.00, 0.02, 0.04, 0.06, 0.08, and 0.10) were successfully synthesized via the sol–gel auto-combustion method, followed by calcination at 1000 °C for 2 h. The influence of Mg substitution on phase formation, crystallite size, microstructural evolution, surface morphology, and magnetic behavior of calcium hexaferrite was systematically investigated.

The structural and magnetic property changes with cation substitution in M-type hexaferrites have been widely investigated but a more comprehensive understanding of the correlation between cation substitution and the resulting property changes is still required. Thus, more systematic investigations are needed to understand how their compositional changes affect their magnetic performance for further advanced technological applications. A detailed characterization of the material has been performed with X-ray diffraction (XRD) spectrometer, Raman spectrometer and vibrating sample magnetometer under applied magnetic field of ±14kOe. The results obtained in turn provide insights into the effect of incorporating Mg in the tailoring of the structural and magnetic properties of M-type calcium hexaferrite for their potential application in advanced magnetic and high frequency devices.

MATERIALS AND METHODS

Chelating agent citric acid was used (as fuel) in the preparation of hexaferrite M type $Ca_{1-x}Mg_xFe_{12}O_{19}$ ($0.00 \leq x \leq 0.10$) by sol-gel auto-combustion process. Chemical reagents were all purchased from Merck. Calcium nitrate ($Ca(NO_3)_2$, 98% Purity), magnesium nitrate hexahydrate ($Mg(NO_3)_2.6H_2O$, 99% Purity), ferric nitrate nonahydrate ($Fe(NO_3)_3.9H_2O$, 99.9% purity), citric acid monohydrate ($C_6H_8O_7.H_2O$, 99.9% purity), and ammonia solution (NH_4OH, 25% 25%) were used as starting materials [33]. Firstly, the metal nitrates were dissolved in deionized water with constant stirring by a magnetic stirrer to ensure the precursor solution is homogeneous. Subsequently citric acid was added in a dropwise manner to the mixture with constant stirring to ensure complexation of the metal ions. Ammonia solution was dropped into the solution to adjust its pH to 7 [34, 35]. The mixture was stirred and heated at 80–100°C continuously for about 3-4 h until the water was removed leaving a viscous dark-brown gel. The product obtained was heated in a hot-air oven at 200-250 °C for 1 h, and a self-propagating combustion process was initiated to produce the powder with a loose and porous structure. Finer particle size was achieved by finely grinding the combustion residue in an agate mortar and pestle to make a homogeneous powder before drying at 110°C for 30 min to remove the moisture. The dried powder was then calcined in air at 1000°C for 3 h to obtain pure magnesium substituted calcium M-type hexaferrite powder which is gray in colour as typical for hexagonal ferrite materials.

Characterization techniques

X-ray Diffraction (XRD) was used to examine the structural properties of the synthesized samples such as phase purity, crystallite size and lattice parameters using an PANalytical X'Pert Pro diffractometer with Cu-Kα radiation (λ=1.5406 Å). Furthermore, Raman spectroscopy measurements

were carried out with a micro-Raman spectrometer (HORIBA Scientific LabRAM HR Evolution, 785 nm laser) to investigate the vibration of the fabricated materials. Field-emission scanning electron microscopy (FESEM) was used for analyzing surface morphology and average particles size employing a TESCAN MIRA3-XMU, Czech Republic. In addition, the magnetic properties of the produced hexaferrite powders were investigated by a vibrating sample magnetometer (VSM, LBKFB) produced by Meghnatis Daghigh Kavir Co. under the applied magnetic field up to ±14 kOe at room temperature.

RESULTS AND DISCUSSION

X-ray Diffraction (XRD)

$Ca_{1-x}Mg_xFe_{12}O_{19}$ ($0.00 \le x \le 0.10$) hexaferrite samples were prepared by calcining the samples at 1000 °C, and the crystal structure and phase purity of the samples were investigated by X-ray diffraction (XRD). The diffraction patterns obtained are shown in Fig. 1. The observed diffraction peaks indexed to the crystallographic planes (006), (107), (114), (202), (109), (214), (303), (2011), (208), (217), and (220) were found to be in good agreement with the standard JCPDS card No. 49-1586 corresponding to the M-type hexagonal structure. Sharp and distinct diffraction peaks can be seen in the X-ray diffraction plots, which indicates high crystallinity for the synthesized samples. Moreover, all peaks are in agreement with the previous studies [36, 37, 38]. The XRD diffractograms showed no secondary phases nor any impurity peaks, suggesting that the single-phase M-type hexagonal ferrite structure was formed successfully [38]. Slightly, it was also noted that the strongest diffraction peak (107) gradually moved to lower Bragg angles as the Mg content (x) increased. This transition is believed to be due to lattice distortion caused by the substitution of Mg^{2+} at the Ca^{2+} lattice sites due to the difference in ionic radius of the two ions (Mg^{2+} = 0.72 Å and Ca^{2+} = 1.00 Å). The shift in peak position found in Table 1 is also indicative of the occurrence of structural distortion after Mg incorporation. Similar behavior has also been reported by Chauhan et al. [7].

Various structural parameters, including the crystallite size (D), lattice constants (a, c, and c/a), unit cell volume (V_{cell}), and X-ray density (ρ_x), were calculated for all powder samples using the following equations [39, 40].

$$D_{=} = \frac{0.9\,\lambda}{\beta \cos\theta} \tag{1}$$

$$\frac{1}{d^2} = \left[\frac{4}{3a^2}\left(h^2 + hk + k^2\right) + \frac{l^2}{c^2}\right] \tag{2}$$

$$V_{cell} = \frac{\sqrt{3}}{2} a^2 c \tag{3}$$

$$\rho_x = \frac{2M}{N_A a^3} \tag{4}$$

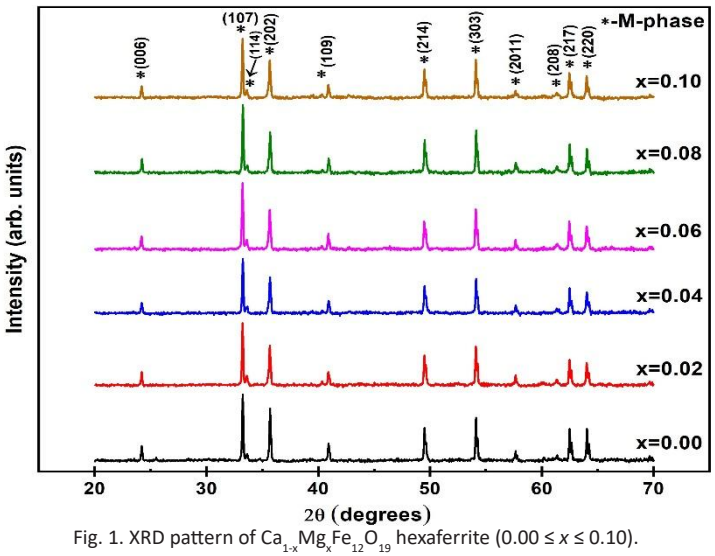

Fig. 1. XRD pattern of $Ca_{1-x}Mg_xFe_{12}O_{19}$ hexaferrite ($0.00 \le x \le 0.10$).

where λ is the wavelength of the X-ray radiation, β represents the full width at half maximum (FWHM) of the diffraction peak, θ is the Bragg angle corresponding to the maximum intensity peak, d is interplanar distance, h, k, and l are Miller indices, M denotes the molecular weight of the sample, and N_A is Avogadro's number.

Table 1 presents the structural properties of the prepared samples. A noticeable decrease in crystallite size was observed with increasing Mg^{2+} substitution, where the crystallite size declined from 71.44 nm (x = 0.00) to 65.79 nm (x = 0.06). After that increased to 68.49 nm (x=0.08) and then decreased to 67.43 nm. This might be due to the difference between the ionic radii of Mg^{2+} (0.72Å) and Ca^{2+} (1.00Å) and produced lattice strain which lead to a reduction in crystallite size. Similar types of result were observed by Shinde et.al. and Khan et al. [36, 41]. The obtained values of the lattice parameters belong to the pure magnetoplumbite phase (a=5.892-5.897Å and c=23.168-23.182 Å) of hexaferrite as reported elsewhere [41]. The lattice constant 'α' approximately remains unchanged while 'c' has shown small variation which can be interpreted from the ionic radii of Mg^{2+} and Ca^{2+}. And also associated with defects and lattice distortion. Similar results were observed by Khobragade et al. [42].

The variation in both lattice parameters and crystallite size provides strong evidence for the successful incorporation of Mg^{2+} ions into the hexaferrite crystal lattice rather than forming secondary impurity phases. The substitution of Ca^{2+} by Mg^{2+} modifies the local structural environment because of the difference in their ionic radii, leading to internal lattice strain and slight distortion within the magnetoplumbite structure. Such structural modifications are commonly observed in substituted M-type hexaferrites and are considered indicative of effective dopant incorporation into the host lattice. According to the structural criterion proposed by Verstegen and Stevels, the M-type hexaferrite phase is stable when the c/a ratio remains below 3.98. In the present work, the calculated c/a values range from 3.926 to 3.933, confirming the preservation of the magnetoplumbite M-type hexagonal structure for all compositions [43]. These results imply that the crystal symmetry of the parent phase remains largely unchanged upon Mg substitution.

Besides, the unit cell volume was found to vary slightly from 699.529 Å3 to 699.570 Å3· The small changes are directly related to the small changes in lattice constants (a and c) due to the incorporation of Mg. Such non-uniform behaviour of the cell volume can be due to the competition among the ionic size mismatch, a local lattice relaxation, and generation of defects during the substitution process. The same type of behavior has been also observed in substituted ferrite systems where the spacing and packing density of the structure are affected by the dopant ions. The X-ray density (ρ_x) was also seen to gradually decrease with increasing Mg^{2+} concentration. This is because the replacement of heavier Ca^{2+} ions with lighter Mg^{2+} ions decreases the molecular weight, which explains this trend. The changes in mass of the molecule are larger than the corresponding changes in the unit cell volume, so that the overall X-ray density decreases with increasing Mg content [38]. This behaviour also helps in the successful substitution and the achievement of

Table 1. Structural parameters for $Ca_{1-x}Mg_xFe_{12}O_{19}$ hexaferrite ($0.00 \le x \le 0.10$).

Comp.	D_{XRD} (nm)	a (Å)	c (Å)	c/a ratio	V (Å^3)	Most Intense Peak Position (degree)	ρ_x (gm/cm^3)
$CaFe_{12}O_{19}$	71.44	5.895	23.174	3.931	699.543	33.213	4.814
$Ca_{0.98}Mg_{0.02}Fe_{12}O_{19}$	69.56	5.896	23.170	3.930	699.529	33.201	4.813
$Ca_{0.96}Mg_{0.04}Fe_{12}O_{19}$	68.78	5.893	23.180	3.929	699.564	33.217	4.812
$Ca_{0.94}Mg_{0.06}Fe_{12}O_{19}$	65.79	5.897	23.168	3.929	699.570	33.194	4.811
$Ca_{0.92}Mg_{0.08}Fe_{12}O_{19}$	68.49	5.892	23.182	3.933	699.556	33.229	4.810
$Ca_{0.90}Mg_{0.10}Fe_{12}O_{19}$	67.43	5.896	23.169	3.926	699.567	33.196	4.809

a single phase of the compositionally modified hexaferrites.

Raman Measurements

As a versatile characterization method, Raman spectroscopy provides valuable information on lattice dynamics, crystal structure ordering, and local bonding environments in ferrites [44]. Theoretically, 42 modes are expected in the Raman spectrum of the hexagonal M-type for which all the modes are Raman active which corresponds to $11A_{1g}$,$14E_{1g}$, and $17E_{2g}$ modes according to the group theoretical analysis. Furthermore, it is expected that the crystal structure will have 30 IR modes and some optically inactive modes of various symmetries [45, 46]. Room-temperature Raman spectra of $Ca_{1-x}Mg_xFe_{12}O_{19}$ ($0.00 \le x \le 0.10$) were obtained within the 100 - 700 cm^{-1} range and are illustrated in Fig. 2. The undoped $CaFe_{12}O_{19}$ sample (x = 0.00) exhibits distinct Raman bands located at approximately 176.77, 191.94, 223.36, 290.45, 413.06, 460.59, 500.55, and 609.58 cm^{-1}. The sharpness and intensity of these modes suggest good crystallization of the hexaferrite phase and low density of structural defects. As the Mg substitution increased, it can be seen that the intensity of the peaks of the Raman spectra increases, and there were also slight wavenumber changes. The changes in the lattice modifications suggest that the lattice structure is under local changes due to the incorporation of Mg^{2+} ions in the $CaFe_{12}O_{19}$ structure. The Fe -

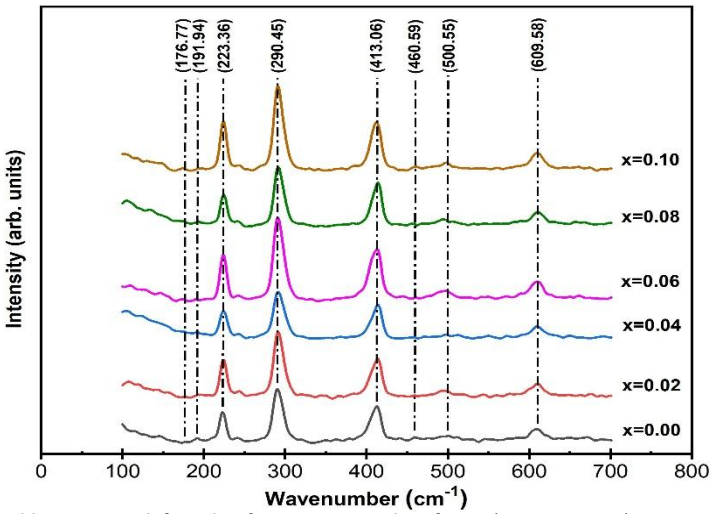

Table 2. Raman shift peaks of $Ca_{1-x}Mg_xFe_{12}O_{19}$ hexaferrite ($0.00 \le x \le 0.10$).

Table 2. Raman shift peaks of $Ca_{1-x}Mg_xFe_{12}O_{19}$ hexaferrite ($0.00 \le x \le 0.10$).

Raman Shift (cm^{-1}) Peaks - $Ca_{1-x}Mg_xFe_{12}O_{19}$ hexaferrite ($0.00 \le x \le 0.10$).						Symmetry	Assigned polyhedral
X=0.00	X=0.02	X=0.04	X=0.06	X=0.08	X=0.10		
176.77	176.77	175.50	175.50	174.24	174.24	E_{1g} [11, 52]	Whole spinel block
191.94	193.20	191.94	191.94	193.20	193.20	E_{1g} [11, 52]	Whole spinel block
223.36	226.62	226.62	226.62	226.62	226.62	E_{1g} [52, 53]	Octahedrahedral
290.45	291.68	291.68	291.68	291.68	291.68	A_{1g} [54, 55]	Octahedrahedral (2a)
413.06	414.25	414.25	413.06	414.25	411.86	E_{2g} [54, 55]	Octahedral 12k dominated
460.59	459.41	459.41	460.59	459.41	460.59	A_{1g} [53, 55]	Octahedrahedral (2a + 12k)
500.55	498.21	498.21	498.21	498.21	499.38	A_{1g} [53, 56]	Octahedrahedral (12k)
609.58	610.73	609.58	609.58	610.73	610.73	A_{1g} [53, 57]	Octahedrahedral (4f2)

O bond characteristics are also changed and the local distortion of the crystal structure is increased by substituting Mg^{2+} ions for Ca^{2+} ions, as the ionic radius of Mg^{2+} is smaller (0.72 Å) than that of Ca^{2+} (1.00 Å) [47], As a result, changes in the force constants of lattices and phonon vibrations appear and cause slight differences in the Raman frequencies. In addition, the incorporation of Mg ions may modify the cation distribution between octahedral and tetrahedral sites, resulting in slight variations in local symmetry and vibrational properties. The gradual broadening of Raman bands with increasing Mg content indicates enhanced phonon scattering and a moderate increase in lattice disorder [11, 48].

The Raman spectra obtained are in accordance with the previously reported spectra of M-type hexaferrite [49]. No other Raman bands attributable to impurity phases or secondary compounds have been found, which is a sign of obtaining a single-phase structure of a hexaferrite. This is in agreement to the XRD result, which also revealed the phase purity of the synthesized compositions. The overall spectral characteristics were almost the same for the various additions of Mg but slight changes in the band positions were noticed, indicating small changes in the vibrational environment brought about by the incorporation of Mg. The same behavior has been observed in substituted ferrite systems, where a substitution by smaller ions alters the bond lengths and the interaction with the lattice, consequently changing the phonon frequencies and modes which are Raman active [50, 51].

A table of Raman spectral parameters obtained from all the samples investigated is summarized in Table 2. The Raman peak intensity was the lowest for the pure $CaFe_{12}O_{19}$ composition while

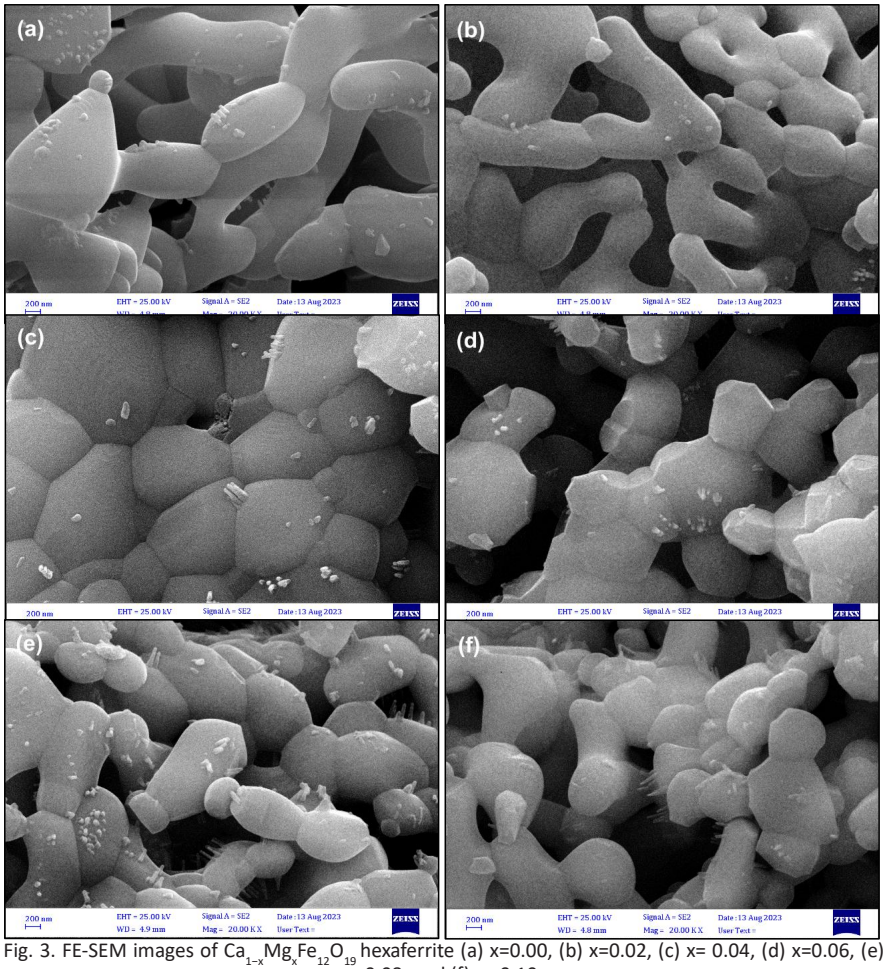

Fig. 3. FE-SEM images of $Ca_{1-x}Mg_xFe_{12}O_{19}$ hexaferrite (a) x=0.00, (b) x=0.02, (c) x= 0.04, (d) x=0.06, (e) x=0.08, and (f) x= 0.10.

a gradual increase in intensity was seen with the introduction of Mg. This behavior could be related to the relaxation of strain and local ordering of the lattice after incorporation of Mg ions. Moderate peak broadening can also be caused by localized defects and microstrain, which can cause some overlap of bands and loss of symmetry. Such structural variations can affect the magnetic exchange interactions and magnetic anisotropy of hexaferrite system [52]. In conclusion, the Raman study revealed that both pure and Mg-substituted calcium hexaferrites possess typical hexagonal M-type structure and the analysis clearly indicated successful incorporation of Mg^{2+} ions in the crystal lattice of the ferrite materials.

Surface morphology and EDX analysis

Fig. 3 a–f shows the FE-SEM images of M-type hexaferrite powders $Ca_{1-x}Mg_xFe_{12}O_{19}$ ($0.00 \leq x \leq 0.10$) prepared by calcination at 1000°C. Particles agglomeration is observed in all samples with a very high level of particle agglomeration, mainly due to the high intrinsic magnetic dipole-dipole interactions between the single domain hexaferrite grains [58]. The micrographs show that the grain shape changes from spherical to platelet to highly faceted polyhedron shape. The observed inhomogeneous and irregular particle size distribution may be attributed to the synthesis kinetics of the sol-gel auto-combustion method.

This fast exothermic combustion process causes a more rapid crystal nucleation and growth process, resulting in a faster self-sustaining combustion process and local differences in combustion time and flame temperature, which leads to differences in the size of the particles that are formed. Very high temperatures and long calcination times are normally required to achieve a fully crystalline and homogenous hexaferrite phase [59]. At lower substitution levels, an insubstantial change in the average particle size is observed, which is very reasonable, given the very small dopant concentrations. With increasing Mg^{2+} substitution, however, an interesting change in grain boundaries and cross sectional geometry are observed. The grains in the pristine sample (x=0) have diffuse and smooth boundaries and are mostly quasi-oval in shape. On another hand, raising the substitution level, a unique crystallization and clear-separation of grain boundaries occurs, especially at (X=0.04 and 0.06). This is a structural refinement that is very closely coupled to ionic radius discrepancies and diffusion kinetics; the modulating effect of ionic radius of the substituting species on the host lattice parameter facilitates localized atomic diffusion pathways, which enhances the mobility of boundaries and grain growth [60, 61]. The grains are thus endowed with more planar, platelet shape which further improves the lattice anisotropy of the synthesized hexaferrites. These highly anisotropic platelets have a tendency to stack and agglomerate into larger cluster networks, which causes the observed particle-size heterogeneity [62, 63].

Competition between various grain growth processes and atomic diffusion pathways control the morphological transitions in these Mg^{2+} -substituted calcium hexaferrites. The abnormality (exaggerated growth) of grains appears at certain doping concentrations, as shown in Fig. 3 (a–f). This suggests that the reaction mechanism is an interface-controlled process in which the velocities of atomic diffusion are low in this system. This diffusion coefficient is strongly dependent on the substitution concentration and the typical M-type hexagonal habit is maintained at low substitution concentrations. As the concentration increases, the sintering kinetic becomes dominated by accelerated atomic diffusion and a change in the morphology was observed from regular hexagonal to irregular and complex polyhedral geometries [64].

This is in agreement to Kang et al. [65], who suggested that with some substitution this driving force towards uniformity of crystal growth weakens, but at the same time localized abnormal grain growth commences creating a population of smaller grains within the matrix and a few irregularly larger crystals.

Fig. 4 (a–f) depicts the Energy-Dispersive X-ray Spectroscopy (EDX) profiles of the Mg^{2+}-substituted M-type calcium hexaferrite samples, confirming elemental preservation and phase purity. The EDX spectra unequivocally reveal the characteristic X-ray emission peaks corresponding to Calcium (Ca), magnesium (Mg), Iron (Fe), and Oxygen (O). Crucially, the total absence of extraneous or unassigned peaks within the spectra confirms that no foreign impurities or secondary crystalline contaminants were introduced during the sol-gel auto-combustion synthesis or subsequent high-temperature calcination stages. Furthermore, the quantitative atomic percentages obtained from the EDX analysis for all synthesized compositions

were systematically compiled within each figure, demonstrating excellent agreement with the nominal chemical compositions.

Magnetic analysis

Fig. 5 presents the room-temperature magnetic hysteresis (M–H) loops of $Ca_{1-x}Mg_xFe_{12}O_{19}$ M-type calcium hexaferrite nanoparticles ($0.00 \leq x \leq 0.10$), investigated using a vibrating sample magnetometer (VSM). The magnetic parameters, including saturation magnetization (M_s), remanent magnetization (M_r), and coercivity (H_c), were extracted from the hysteresis loops [66], and are summarized in Table 3. The obtained M_s and M_r values were found to vary within the ranges of 1.030-1.637 emu/g and 0.337-0.776 emu/g, respectively. A gradual enhancement in both saturation and remanent magnetization was observed with increasing Mg substitution content. This magnetic enhancement may be associated with the redistribution of Mg^{2+} ions among the crystallographic sublattices of the M-type hexaferrite structure, leading to modifications in the superexchange interactions between Fe^{3+} ions at different lattice sites. The increase in magnetization also suggests improved magnetic ordering and indicates the soft magnetic characteristics of the synthesized nanoparticles.

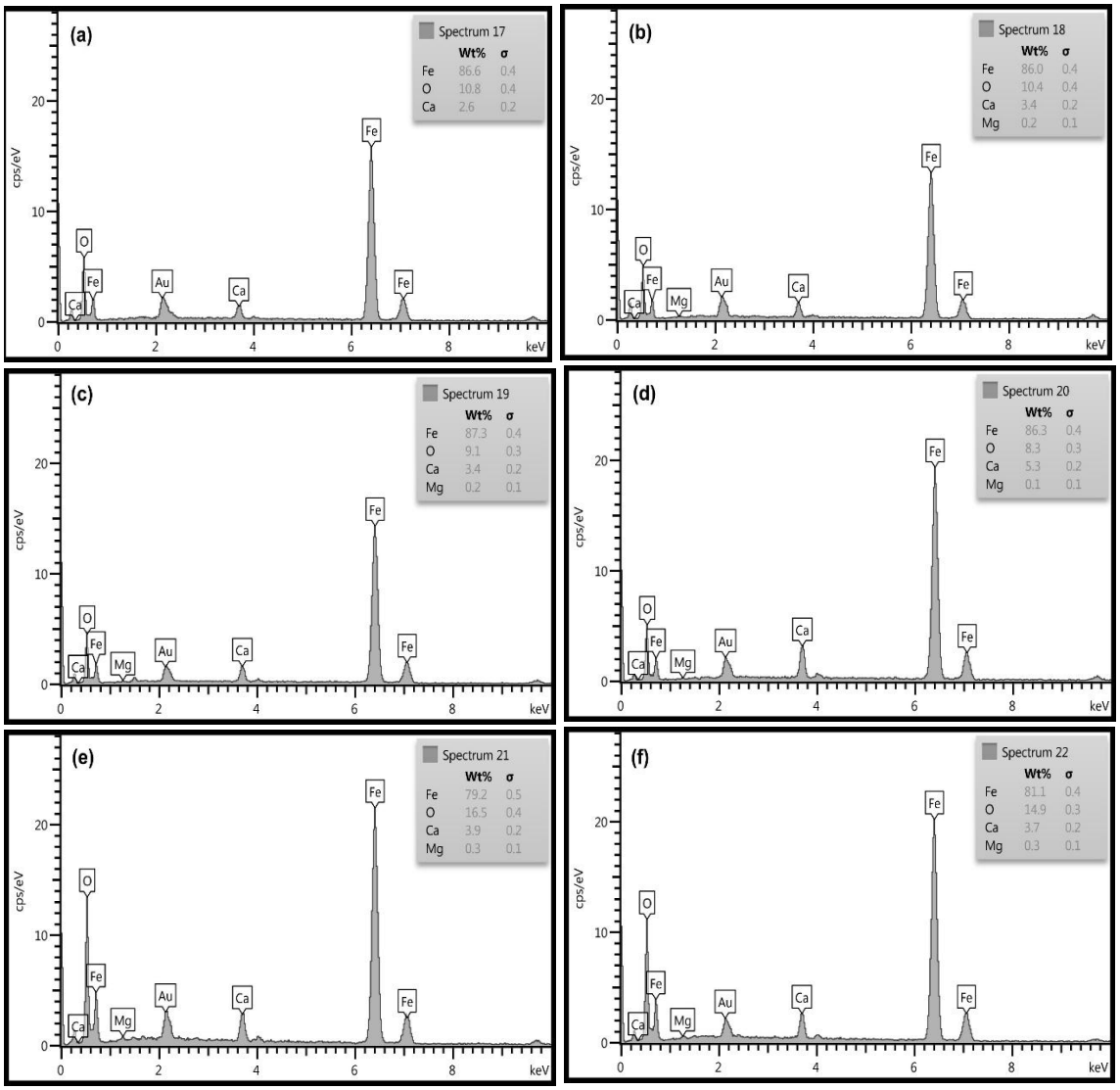

Fig. 4.EDX spectra of $Ca_{1-x}Mg_xFe_{12}O_{19}$ hexaferrite (a) x=0.00, (b) x=0.02, (c) x= 0.04, (d) x=0.06, (e) x=0.08, and (f) x= 0.10.

Furthermore, the observed magnetic behavior can be attributed to variations in cation occupancy and spin alignment within the hexaferrite lattice, which in turn directly affect the net magnetic moment of the material. The relatively low coercivity values further confirm the soft magnetic nature of the prepared samples, indicating their potential suitability for magnetic and microwave-related applications. Similar findings have been previously reported by Shinde et al. [38] for Ni-substituted Ca-M hexaferrite nanoparticles, $CaNi_xFe_{12-x}O_{19}$ (x=0.5,1.0,1.5,2.0), where both M_s and M_r increased systematically with increasing Ni concentration. Their reported values ranged from 8.845–26.055 emu/g for M_s and 1.884–8.426 emu/g for M_r, confirming that divalent ion.

The coercivity (H_c) values of the as-prepared nanoparticles were found to lie within the range

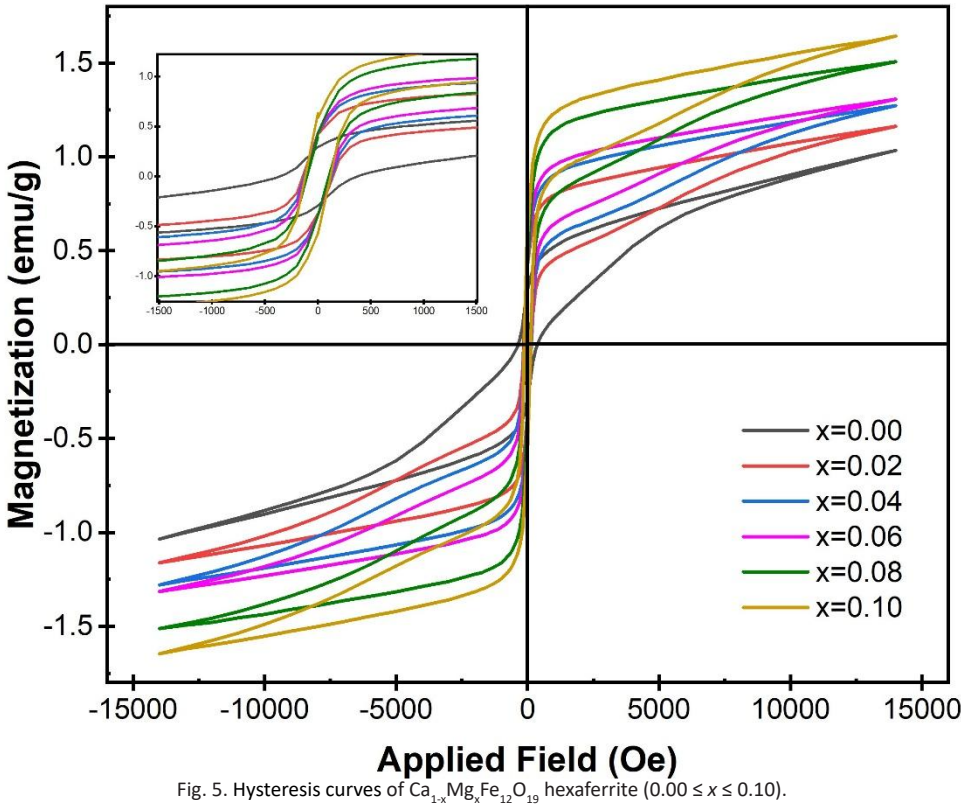

Fig. 5. Hysteresis curves of $Ca_{1-x}Mg_xFe_{12}O_{19}$ hexaferrite ($0.00 \le x \le 0.10$).

Table. 3 Magnetic parameters of $Ca_{1-x}Mg_xFe_{12}O_{19}$ hexaferrite ($0.00 \le x \le 0.10$).

Sample	Ms (emu/g)	Mr (emu/g)	Hc (Oe)	Mr/Ms
$CaFe_{12}O_{19}$	1.030	0.337	400.274	0.327
$Ca_{0.98}Mg_{0.02}Fe_{12}O_{19}$	1.162	0.522	192.131	0.449
$Ca_{0.96}Mg_{0.04}Fe_{12}O_{19}$	1.272	0.574	128.087	0.451
$Ca_{0.94}Mg_{0.06}Fe_{12}O_{19}$	1.305	0.592	128.087	0.453
$Ca_{0.92}Mg_{0.08}Fe_{12}O_{19}$	1.501	0.648	128.087	0.431
$Ca_{0.90}Mg_{0.10}Fe_{12}O_{19}$	1.637	0.776	128.087	0.474

of 128.087-400.274 Oe. A significant reduction in coercivity was observed with increasing Mg content in the Ca-based hexaferrite samples, where H_c decreased from 400.274 Oe for x = 0.00 to 192.131 Oe at x = 0.02, followed by a nearly stable value of approximately 128.087 Oe for the higher Mg concentrations. This behavior is consistent with previously reported studies on hexaferrite systems [67, 68].

The observed decrease in coercivity may be attributed to changes in magnetocrystalline anisotropy and particle size, both of which are known to significantly influence the magnetic properties of ferrite materials [69]. In particular, Mg substitution can reduce the magnetocrystalline anisotropy of the hexaferrite structure while simultaneously promoting particle growth. These effects facilitate domain wall motion, thereby leading to a reduction in coercivity. In summary, as Mg content increases, H_c decreases more, further demonstrating the trend towards a softer magnetic character. Thus, the decrease in coercivity (H_c) with increasing Mg substitution is mainly due to the increase in particle size and the reduction in magnetocrystalline anisotropy that accompanies it. The motion of the domain wall in this case is easier as the particle size increases and so the magnetic field required to flip the magnetisation is decreased. In Ni- and Zn-substituted barium hexaferrites [68], where the cation substitution was found to have a considerable effect on the anisotropy and magnetic domain dynamics, the results are reported. Furthermore, Singh et al. [70] studied the M-type hexagonal ferrite nanoparticles and found that the magnetic parameters changes are highly correlated with the difference in particle size of the different samples produced. They also showed that particle size alteration causes a direct change in the magnetic properties because of the change in the magnetic domain configuration and microstructure.

Similar behavior was found in the current M-type hexagonal ferrite nanoparticles, leading to the conclusion that the evolution of microstructures is important for the magnetic response of the materials prepared. Furthermore, the prepared hexagonal ferrite powders showed low magnetic coercivity which is a significant criterion characterizing the magnetic stability and soft magnetic property. The synthesized nanomaterials are found to have desirable magnetic properties for high frequency and electromagnetic applications, due to their improved resistance to spontaneous demagnetization and magnetic response.

Squareness ratio M_r/M_s is a typical criterion for multi magnetic domains materials. The values in Table 2 (between 0.327 and 0.431) support the multi-domain nature of all the synthesized samples [71, 72].

The obtained values further indicate that the prepared materials have potential applicability in magnetic recording technologies, similar to other ferrite materials, the ratio of M_r/M_s below 0.5 generally shows good recording characteristics [73]. The graph of variations in M_s, M_r, M_r/M_s and H_c of M-type hexaferrite nanoparticles is shown in Fig. 6. The observed changes in the magnetic parameters are also associated with the redistribution of cations between the tetrahedral and octahedral crystallographic sites within the hexaferrite lattice. Ca^{2+} and Mg^{2+} ions have ionic radii of approximately 1.00 Å and 0.72 Å, respectively. and this difference plays an important role in site occupancy and lattice distortion. Incorporation of Mg^{2+} ions into the calcium hexaferrite structure can create local cation vacancies and cause the distribution of Fe^{3+} among the available crystallographic sites to change, which can strengthen the magnetic interactions in the material. However, due to the smaller ionic radius, Mg^{2+} can be incorporated successfully into the host lattice, thereby enhancing the nanoparticles' saturation magnetization and remanent magnetization [73]. Moreover, the magnetic properties of hexaferrite are very sensitive to many structural parameters such as occupancy of the cation positions, lattice strain, superexchange interactions and magnetic moments of the host and substituted ions [74]. Akhtar et al. [75] described the cation distribution in M-type hexagonal ferrites, and interestingly, it was found that the Fe ions reside in tetrahedral, octahedral and trigonal bipyramidal positions, while the Ca ions are more likely to reside in the 2d crystallographic positions. In this structure, the magnetic spins on some of the octahedral and tetrahedral sites are antiparallel, whereas spins attached to the 2a, 2b and 12k sites are parallel, giving rise to the ferrimagnetic properties of the hexaferrite system. According to ligand field theory, the magnetic characteristics of ferrites are closely related to the occupation of octahedral and tetrahedral sites within the crystal lattice. Due to its divalent nature and relatively high electronegativity, Mg^{2+} ions preferentially

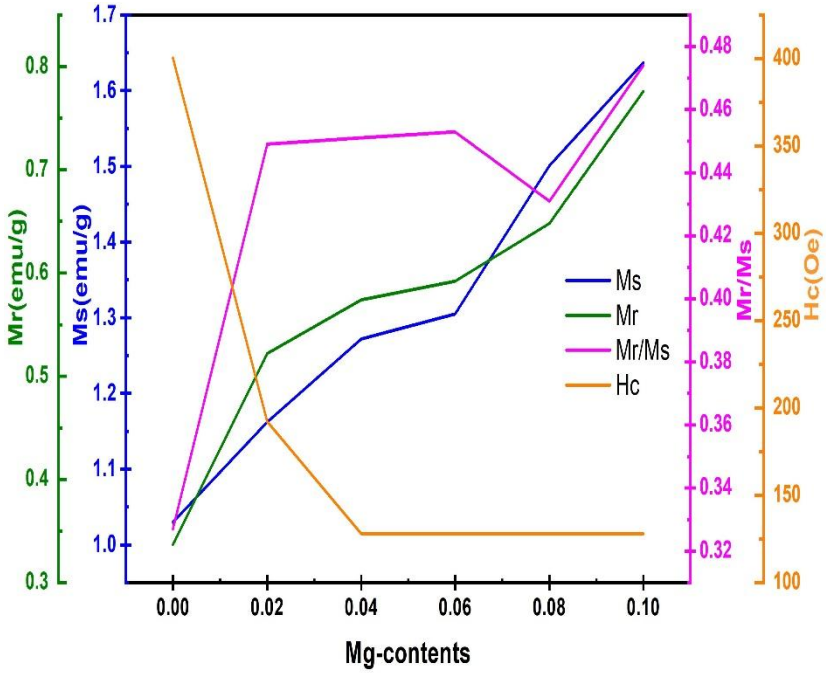

Fig. 6. Variation M_s, M_r, M_r/M_s and H_c for Mg-substituted calcium hexagonal ferrites at different Mg contents.

occupy octahedral sites by partially replacing Ca^{2+} ions. Such substitution modifies the Fe^{3+}-O^{2-}-Fe^{3+} superexchange pathways and consequently alters the overall magnetic response of the material. Therefore, the dopant ions play a crucial role in tailoring the magnetic properties of hexaferrite nanoparticles [76].

CONCLUSION

Mg-substituted calcium M-type hexaferrite nanoparticles ($Ca_{1-x}Mg_xFe_{12}O_{19}$) were successfully synthesized via the sol–gel auto-combustion method, yielding a highly crystalline single-phase hexagonal structure. The incorporation of Mg^{2+} ions caused slight lattice distortion and a reduction in crystallite size due to the ionic radius mismatch between Ca^{2+} and Mg^{2+} ions, while preserving the magnetoplumbite structure. Raman analysis confirmed successful Mg incorporation through slight shifts in the characteristic vibrational modes and modifications in the local Fe–O bonding environment. FE-SEM observations revealed particle agglomeration and a gradual morphological transformation from quasi-spherical grains to platelet-like and polyhedral structures with increasing Mg concentration, whereas EDX analysis verified the compositional purity of the synthesized samples. Magnetic measurements demonstrated enhanced soft magnetic behavior, where saturation and remanent magnetization increased, while coercivity decreased significantly to nearly 128 Oe, confirming improved magnetic response after Mg substitution. In addition, the squareness ratio confirmed the single-domain magnetic nature of the prepared nanoparticles. Overall, Mg substitution effectively tailored the structural and magnetic characteristics of calcium hexaferrites, making them promising materials for microwave absorption, electromagnetic shielding, and high-frequency magnetic applications.

ACKNOWLEDGEMENTS

The authors express their sincere gratitude to the University of Diyala, College of Science, Department of Physics, Iraq, and the University of Garmian, College of Education, Department of Physics, Kurdistan Region, Iraq, for their generous academic and institutional support. Special appreciation is also extended to the DeyPetronic Center, Tehran, Iran, for their invaluable technical assistance and contribution to the experimental procedures and laboratory analyses, which played a crucial role in the successful completion of this research.

CONFLICT OF INTEREST

The authors declare that there is no conflict of interests regarding the publication of this manuscript.

REFRENCES

1. Ahmed HS, Sijo AK, Mohammad AM, Al-Jaf HSA, Ahmed BH, Mazurenko J. Design and Development of Ferrite-TiO_2 Nanocomposites with Tunable Magnetic Properties. East European Journal of Physics. 2025(4):454-460.
2. Ahmed HS, Hussen SA, Mohammad AM. Synthesis and characterization of $Zn_{0.8}Co_{0.2}Fe_2O_4$ ferrite nanoparticles: Magnetic and structural insights. J Sol-Gel Sci Technol. 2025;115(1):17-29.
3. Tarkhany AR, Sijo AK, Mohammad AM, Ahmed HS, Ahmed BH, Al-Jaf HSA. Tailoring magnetic properties of CoNi-Ferrite/SiO_2 nanocomposite. Discover Electronics. 2026;3(1).
4. Mubarak TH, Jumaa MB, Mohammad AM. Structural, magnetic, and antibacterial properties of $Ni_{1-x}Cu_xFe_2O_4$ nanocomposites: influence of Cu substitution. Appl Phys A. 2025;131(10).
5. Joshi H, Ruban Kumar A. Magnetic and dielectric response of M-type barium hexaferrite. J Indian Chem Soc. 2022;99(9):100646.
6. Verma S, Singh A, Godara SK, Ahmed J, Alshehri SM, Singh M. Ca-induced changes in the crystal structure and magnetic properties of barium hexaferrite. Bull Mater Sci. 2023;46(4).
7. Chauhan CC, Kagdi AR, Jotania RB, Upadhyay A, Sandhu CS, Shirsath SE, et al. Structural, magnetic and dielectric properties of Co-Zr substituted M-type calcium hexagonal ferrite nanoparticles in the presence of α-Fe_2O_3 phase. Ceram Int. 2018;44(15):17812-17823.
8. Jotania RB, Khomane RB, Chauhan CC, Menon SK, Kulkarni BD. Synthesis and magnetic properties of barium–calcium hexaferrite particles prepared by sol–gel and microemulsion techniques. J Magn Magn Mater. 2008;320(6):1095-1101.
9. Qiu J, Shen H, Gu M. Microwave absorption of nanosized barium ferrite particles prepared using high-energy ball milling. Powder Technol. 2005;154(2-3):116-119.
10. Rane VA, Meena SS, Gokhale SP, Yusuf SM, Phatak GJ, Date SK. Synthesis of Low Coercive $BaFe_{12}O_{19}$ Hexaferrite for Microwave Applications in Low-Temperature Cofired Ceramic. J Electron Mater. 2013;42(4):761-768.
11. Seyyed Ebrahimi SA. The Powder and Bulk Magnetic Properties of Strontium Hexaferrite Substituted by La and Nd. Key Eng Mater. 2007;280-283:467-470.
12. Chawla SK, Mudsainiyan RK, Meena SS, Yusuf SM. Sol–gel synthesis, structural and magnetic properties of nanoscale M-type barium hexaferrites $BaCo_xZr_xFe_{(12-2x)}O_{19}$. J Magn Magn Mater. 2014;350:23-29.
13. Mudsainiyan RK, Chawla SK, Meena SS. Correlation between site preference and magnetic properties of Co–Zr doped $BaCo_xZr_xFe_{(12-2x)}O_{19}$ prepared under sol–gel and citrate precursor sol–gel conditions. J Alloys Compd. 2014;615:875-881.
14. Chawla SK, Meena SS, Kaur P, Mudsainiyan RK, Yusuf SM. Effect of site preferences on structural and magnetic switching properties of CO–Zr doped strontium hexaferrite $SrCo_xZr_xFe_{(12-2x)}O_{19}$. J Magn Magn Mater. 2015;378:84-91.
15. Kaur P, Chawla SK, Meena SS, Yusuf SM, Pubby K, Narang SB. Modulation of physico-chemical, magnetic, microwave and electromagnetic properties of nanocrystalline strontium hexaferrite by Co-Zr doping synthesized using citrate precursor sol-gel method. Ceram Int. 2017;43(1):590-598.
16. Alsmadi AM, Bsoul I, Mahmood SH, Alnawashi G, Prokeš K, Siemensmeyer K, et al. Magnetic study of M-type doped barium hexaferrite nanocrystalline particles. J Appl Phys. 2013;114(24).
17. K AM, Selvi KT, Priya M. Effect of Co and Sm Substitutions on the Magnetic Interactions of M-Type Strontium Hexaferrite Nanoparticles. Journal of Superconductivity and Novel Magnetism. 2019;33(3):713-720.
18. Himanshi, Jasrotia R, Prakash J, Verma R, Thakur P, Kandwal A, et al. Synthesis, characterization, and applications of doped barium hexaferrites: A review. Physica B: Condensed Matter. 2023;667:415202.
19. Mohammed J, Suleiman AB, Hafeez HY, Carol T TT, Sharma J, Bhadu GR, et al. Effect of heat-treatment on the magnetic and optical properties of $Sr_{0.7}Al_{0.3}Fe_{11.4}<Mn_{0.6}O_{19}$. Materials Research Express. 2018;5(8):086106.
20. Mironovich AY, Kostishin VG, Shakirzyanov RI, Mukabenov AA, Melnikov SA, Ril AI, et al. Effect of the Fe/Ba and Fe/Sr ratios on the phase composition, dielectric properties and magnetic characteristics of M-type hexaferrites prepared by the hydrothermal method. J Solid State Chem. 2022;316:123625.
21. Zhuravlev VA, Itin VI, Minin RV, Lopushnyak YM, Svetlichnyi VA, Lapin IN, et al. Influence of different organic fuels on the phase composition, structure parameters and magnetic properties of hexaferrites BaFe12O19 synthesized by the sol-gel combustion. J Alloys Compd. 2019;771:686-698.
22. Masoudpanah SM, Seyyed Ebrahimi SA. Effect of pH value on the structural and magnetic properties of nanocrystalline strontium hexaferrite thin films. J Magn Magn Mater. 2011;323(21):2643-2647.
23. Shaker DM, Ahmed RR, Mohammad AM, Mubarak TH, Mohamed IH. Synthesis and Characterization of $CoZnFe_2O_4$ Ferrite Nanoparticles by Co-precipitation Method for Biomedical Applications. Passer Journal of Basic and Applied Sciences. 2024;6(2):488-493.
24. Banaj L, Agrawal S. Dielectric behavior of Zr4+ doped $MgFe_2O_4$ spinel ferrite synthesized by solid-state reaction method. Current Applied Physics. 2023;56:47-65.
25. Zhang C, Liu X, Rehman KMU, Liu C, Li H, Meng X. Structural and properties of hydrothermally synthesised M-type hexaferrites. Journal of Materials Science: Materials in Electronics. 2016;28(6):4593-4597.
26. Ramírez-Ayala MF, Guerrero AL, Herrera-González AM, Pérez-Juache TJ, López-Juárez R, Elizalde-Galindo JT, et al. Study of neodymium addition on the magnetic and structural properties of strontium hexaferrite synthesized by the Pechini method. J Magn Magn Mater. 2023;582:170985.
27. Ahmed HS, Saeed SR, Mohammad AM. Structural, magnetic, and antibacterial properties of $Co_{1-x}Ni_xCd_{0.2}Fe_2O_4$ ferrite nanocomposites: The role of nickel substitution. Appl Phys A. 2026;132(4).
28. Deshpande AD, Rewatkar KG, Nanoti VM. Study of Morphology and Magnetic Properties of Nanosized Particles of Zirconium – Cobalt Substituted Calcium Hexaferrites. Materials Today: Proceedings. 2017;4(11):12174-12179.
29. Husain K, Ullah Asif S, Abdu Musad Saleh E, Althomali RH, Moharam MM, Hasan I. Samarium substituted M-type Ca-hexaferrites: Structural and magnetic features. Inorg Chem Commun. 2024;165:112493.
30. Ijaz M, Shaheen N, Saeedi AM, Solre GFB, Abdu Musad

Saleh E, Kassem AF, et al. Cu^{2+}/Dy^{3+} dual doped calcium based $Ca_{1-x}Cu_xFe_{12-x}Dy_xO_{19}$ hexaferrites: Microstructural and magnetic properties for magnetic applications. Materials Science and Engineering: B. 2024;304:117341.
31. Al-Dossari M, Anwar T, Saeedi AM, Althomali RH, Solre GFB, Ullah Asif S, et al. Structural and magnetic aspects of aluminium substituted dual lanthanum and calcium based hexaferrite nanoparticles for magnetic applications. Materials Science and Engineering: B. 2024;310:117709.
32. Kumar S, Bhat SA, Chaurasiya S, Lone GA, Rashid A, Sharma PK, et al. Investigation on the structural, morphological and magnetic properties of Ca1-Eu Fe12-Ti O19 hexaferrite system. Solid State Sciences. 2023;145:107337.
33. Majed Saheb H, Heydaryan K, Khojasteh H, Aspoukeh P, Mohammadalizadeh M, Sadat Fini M, et al. Sol–gel-derived $ErFeO_3/Fe_3O_4$/graphene oxide hybrid nanocomposites: green auto-combustion synthesis, structural evolution, and visible-light functional performance. J Sol-Gel Sci Technol. 2026;118(3).
34. Ahmed HS, Saeed SR, Mohammad AM. Effect of barium titanate content on the magnetic, dielectric, and antibacterial properties of $(x)BaTiO_3+(1-x)CoCdFe_2O_4$ nanocomposites. Emergent Materials. 2026;9(5).
35. Ahmed HS, Mohammad AM, Qader IN, Babakr KA, Al-Jaf HSA, Ali BT, et al. Silica-Induced Structural Refinement and Magnetic Dilution of $NiFe_2O_4$ Nanocomposites. J Electron Mater. 2025;55(3):2832-2844.
36. Shinde VS, Dahotre SG, Singh LN. Synthesis and characterization of aluminium substituted calcium hexaferrite. Heliyon. 2020;6(1):e03186.
37. Bhadan M, Pangotra A, Parth, Sood AK, Ahmed J, Alshehri SM, et al. Synthesis and characterization of Ni^{2+}- Zr^{4+} doped Ba-Ca M-type hexaferrites using sol-gel auto-combustion method. Chemical Physics Impact. 2024;9:100742.
38. Shinde VS, Dahotre SG, Singh LN. Study of Structural and Magnetic Properties of Ni Substituted M Type Calcium Hexaferrite. Integrated Ferroelectrics. 2021;213(1):122-136.
39. Abdulhussein HJ, Mohammad AM. Zn-substituted CuMn ferrite nanoparticles for enhanced NO2 gas sensing: synthesis, characterization, and high-performance. J Sol-Gel Sci Technol. 2025;116(3):1764-1774.
40. Atkare SS, Shirsath SE, Batoo KM, Ijaz MF, Deshmukh VJ, Kadam RH, et al. Enhancing the magnetic and dielectric properties of M type strontium hexaferrite nanoparticles via aluminum substitution: a sol-gel synthesis approach. J Sol-Gel Sci Technol. 2025;116(1):421-433.
41. Khan HM, Islam MU, Xu Y, Asif Iqbal M, Ali I. Structural and magnetic Properties of TbZn-substituted calcium barium M-type nano-structured hexa-ferrites. J Alloys Compd. 2014;589:258-262.
42. C. L. Khobaragade SBDSVS, K. G. R CLKSBDSVS, K. G R. Improvement of the Structural, Electrical And Magnetic Properties Of Calcium W-Type Hexaferrite Nano Sized Powders Using Co-Precipitation Method. International Journal of Researches in Biosciences and Agriculture Technology. 2015.
43. Rehman KMU, Liu X, Yang Y, Feng S, Tang J, Ali Z, et al. Structural, morphological and magnetic properties of $Sr_{0.3}La_{0.48}Ca_{0.25}n[Fe(2-0.4/n)O_3]Co_{0.4}$ (n = 5.5, 5.6,5.7,5.8, 5.9, 6.0) hexaferrites prepared by facile ceramic route methodology. J Magn Magn Mater. 2018;449:360-365.
44. Wei Y, Sun X, Meng X, Li Z, Zhang L, Zhou K, et al. Enhancing the properties of Cd-free MgZnS buffer for solar cells by co-sputtering ZnS and Mg targets. Materials Today Communications. 2024;39:108766.
45. Nethala GP, Tadi R, Gajula GR, Chidambara Kumar KN, Veeraiah V. Investigations on the structural, magnetic and mossbauer properties of cerium doped strontium ferrite. Physica B: Condensed Matter. 2018;550:136-144.
46. Zhao WY, Wei P, Wu XY, Wang W, Zhang QJ. Lattice vibration characterization and magnetic properties of M-type barium hexaferrite with excessive iron. J Appl Phys. 2008;103(6).
47. Auwal IA, Baykal A, Güner S, Sertkol M, Sözeri H. Magneto-optical properties $BaBi_xLa_xFe_{12-2x}O_{19}$ ($0.0\leq x\leq 0.5$) hexaferrites. J Magn Magn Mater. 2016;409:92-98.
48. Kumar S, Supriya S, Kar M. Correlation between temperature dependent dielectric and DC resistivity of Cr substituted barium hexaferrite. Materials Research Express. 2017;4(12):126302.
49. Kreisel J, Lucazeau G, Vincent H. Raman study of substituted barium ferrite single crystals, $BaFe_{12-2x}Me_xCoxO_{19}$ (Me=Ir, Ti). J Raman Spectrosc. 1999;30(2):115-120.
50. Chen X-B, Minh Hien NT, Han K, Chul Sur J, Sung NH, Cho BK, et al. Raman studies of spin-phonon coupling in hexagonal $BaFe_{12}O_{19}$. J Appl Phys. 2013;114(1).
51. Anbarasu V, Md Gazzali PM, Karthik T, Manigandan A, Sivakumar K. Effect of divalent cation substitution in the magnetoplumbite structured BaFe12O19 system. Journal of Materials Science: Materials in Electronics. 2012;24(3):916-926.
52. Kumar S, Supriya S, Pandey R, Pradhan LK, Singh RK, Kar M. Effect of lattice strain on structural and magnetic properties of Ca substituted barium hexaferrite. J Magn Magn Mater. 2018;458:30-38.
53. Mustofa S, Rizaldy R, Adi WA. Study of Raman Spectra of Aluminum Powder-Substituted Barium Hexaferrite (BaM) $BaFe_{12-x}Al_xO_{19}$ as a Result of Solid State Reaction Process. IOP Conference Series: Materials Science and Engineering. 2017;202:012040.
54. Chaurasiya S, Kumar S, Lone GA, Kumar A, Sankhala K, Nazir N, et al. Influence of Gd and Ni doping on the structural, morphological, and magnetic properties of M-type calcium hexaferrite. New J Chem. 2024;48(12):5144-5159.
55. Hien NTM, Han K, Chen XB, Sur JC, Yang IS. Raman scattering studies of spin-waves in hexagonal $BaFe_{12}O_{19}$. J Raman Spectrosc. 2012;43(12):2020-2024.
56. Ateia EE, Yasser Y, Shafaay AS. Multi-substituted barium hexaferrite with magnetoplumbite structure for microwave high-frequency applications. J Sol-Gel Sci Technol. 2025;115(1):98-114.
57. Roohani E, Arabi H, Sarhaddi R, Sudkhah S. M-Type Strontium Hexaferrite Nanoparticles Prepared by Sol-Gel Auto-combustion Method: The Role of Co Substitution in Structural, Morphological, and Magnetic Properties. Journal of Superconductivity and Novel Magnetism. 2017;30(6):1599-1608.
58. Mohammed J, Hafeez HY, Tchouank Tekou Carol T, Ndikilar CE, Sharma J, Maji PK, et al. Structural, dielectric, and magneto-optical properties of Cu^{2+}-Er^{3+} substituted nanocrystalline strontium hexaferrite. Materials Research Express. 2019;6(5):056111.
59. Almessiere MA, Slimani Y, El Sayed HS, Baykal A. Structural and magnetic properties of Ce-Y substituted strontium nanohexaferrites. Ceram Int. 2018;44(11):12511-12519.
60. Yuping L, Daxin B, Zhangzhong W, Zhang Y, Lizhao C,

Guangcheng Z, et al. Fabrication of M-type ferrites with high La-Co concentration through Ca^{2+} doping. J Alloys Compd. 2018;734:130-135.
61. Trusov LA, Gorbachev EA, Lebedev VA, Sleptsova AE, Roslyakov IV, Kozlyakova ES, et al. Ca–Al double-substituted strontium hexaferrites with giant coercivity. Chem Commun. 2018;54(5):479-482.
62. Moon K-S, Kang Y-M. Structural and magnetic properties of Ca-Mn-Zn-substituted M-type Sr-hexaferrites. J Eur Ceram Soc. 2016;36(14):3383-3389.
63. Peng L, Li L, Wang R, Hu Y, Tu X, Zhong X. Effect of La–CO substitution on the crystal structure and magnetic properties of low temperature sintered Sr1−La Fe12−Co O19 (x=0–0.5) ferrites. J Magn Magn Mater. 2015;393:399-403.
64. Kim M, Lee K, Bae C, Kim J. Magnetic and morphological properties of Ca substituted M-type hexaferrite powders synthesized by the molten salt method. AIP Advances. 2021;11(5).
65. Kang SJL, Lee MG, An SM. Microstructural Evolution During Sintering with Control of the Interface Structure. J Am Ceram Soc. 2009;92(7):1464-1471.
66. Digest Journal of Nanomaterials and Biostructures.
67. Dhage VN, Mane ML, Babrekar MK, Kale CM, Jadhav KM. Influence of chromium substitution on structural and magnetic properties of $BaFe_{12}O_{19}$ powder prepared by sol–gel auto combustion method. J Alloys Compd. 2011;509(12):4394-4398.
68. Behera P, Ravi S. Effect of Ni doping on structural, magnetic and dielectric properties of M-type barium hexaferrite. Solid State Sciences. 2019;89:139-149.
69. C Alange R. Structural and Magnetic Properties of Zn^{2+} Doped Cobalt Ferrite Nanoparticles Synthesized by Sol-gel Auto Combustion Method. International Journal of Science and Research (IJSR). 2021;10(7):981-983.
70. Singh C, Narang SB, Hudiara IS, Bai Y, Marina K. Hysteresis analysis of Co–Ti substituted M-type Ba–Sr hexagonal ferrite. Mater Lett. 2009;63(22):1921-1924.
71. Gholizadeh A, Banihashemi V. Structural, magnetic, and dielectric properties of $Sr_{1-x}CaxFe_{12}$ − $ySmyO_{19}$ (x = 0.00–0.20, y = 0.00–0.05) hexaferrite. Journal of Materials Science: Materials in Electronics. 2023;34(6).
72. Mohammad AM, Saleh AM, Ahmed BH, Azeez YH, Fatah SK, Mehranfar H. Comprehensive study on the temperature-dependent properties of $Co_{0.5}Mg_{0.5}FeCrO_4$ ferrite nanoparticles: experimental and theoretical analyses. J Sol-Gel Sci Technol. 2024;116(1):303-318.
73. Mamatha C, Krishnaiah M, Sreedhar B. Enhancement Of Magnetic Properties Of Calcium Hexaferrites With Aluminium Substitution. Procedia Engineering. 2017;215:130-135.
74. Yousaf M, Nazir S, Hayat Q, Akhtar MN, Akbar M, Lu Y, et al. Magneto-optical properties and physical characteristics of M-type hexagonal ferrite (Ba1-xCaxFe11.4Al0.6O19) nanoparticles (NPs). Ceram Int. 2021;47(8):11668-11676.
75. Akhtar MN, Javed S, Ahmad M, Sulong AB, Khan MA. Sol gel derived MnTi doped Co2 W-type hexagonal ferrites: Structural, physical, spectral and magnetic evaluations. Ceram Int. 2020;46(6):7842-7849.
76. Ali I, Islam MU, Awan MS, Ahmad M, Asif Iqbal M. Structural, Electrical, and Microstructure Properties of Nanostructured Calcium Doped Ba-Hexaferrites Synthesized by Sol-Gel Method. Journal of Superconductivity and Novel Magnetism. 2013;26(11):3277-3286.